Structural domain and finite-size effects of the antiferromagnetic S=1/2 honeycomb lattice in $InCu_{2/3}V_{1/3}O_3$

A. Möller,[1] U. Löw,[2] T. Taetz,[1] M. Kriener,[3,*] G. André,[4] F. Damay,[4] O. Heyer,[3] M. Braden,[3] and J. A. Mydosh[3]
[1]*Institut für Anorganische Chemie, Universität zu Köln, 50939 Köln, Germany*
[2]*Technische Universität Dortmund, Theoretische Physik I, 44221 Dortmund, Germany*
[3]*II. Physikalisches Institut, Universität zu Köln, 50937 Köln, Germany*
[4]*Laboratoire Léon Brillouin, CEA/CNRS, F-91191 Gif-sur-Yvette Cedex, France*
(Received 5 March 2008; revised manuscript received 13 June 2008; published 18 July 2008)

The compound $InCu_{2/3}V_{1/3}O_3$ has been studied by spectroscopy in the IR, near-infrared, and visible regions. X-ray and neutron diffraction indicate two-dimensional (2D) structural order of magnetic Cu^{2+} ($S=1/2$) ions on a honeycomb lattice with nonmagnetic V^{5+} ions complementing the hexagonal layer. Superstructure reflections observed by neutron diffraction reveal the presence of this 2D structural Cu/V order in domains of approximately 300 Å with a disordered stacking along the *c* axis. Specific-heat, thermal-expansion, and neutron-diffraction experiments gave no signs of a three-dimensional long-range magnetic order. Strong 2D magnetic correlations seem to persist down to low temperatures, providing evidence of an incipient Néel-type ground state on this hitherto rarely studied lattice geometry in $InCu_{2/3}V_{1/3}O_3$. Magnetic correlations in these structural domains are compared with continuous time quantum-Monte Carlo calculations of the specific heat and in particular of the spin-spin-correlation length.

DOI: 10.1103/PhysRevB.78.024420 PACS number(s): 61.66.Fn

I. INTRODUCTION

Since the discovery of high-temperature superconductivity in the cuprates, the study of quasi-two-dimensional magnetic systems has developed into a vast subfield of modern solid-state research. While in the first few years following the discovery by Bednorz and Müller,[1] $S=1/2$ systems on a cubic lattice have been in the center of attention; more recently also other geometries have shown a rich variety of interesting and unexpected behavior. Often this arises from geometrical frustration most evident in triangular spin lattices.[2] One special variety of this geometry is the honeycomb net, which has not yet been studied in great detail. Like the square lattice the honeycomb lattice is not frustrated for antiferromagnetic (AF) nearest-neighbor interactions but, due to the smaller coordination number of three, quantum fluctuations are expected to play a larger role. Experimentally there are only a few examples of materials where the electron spins are located in a two-dimensional honeycomb lattice, however such diverse phenomena as spin-glass states,[3,4] Kosterlitz-Thouless transitions,[5,6] or superconductivity[7,8] have been reported.

We present here powder x-ray and neutron powder diffraction (NPD), as well as specific-heat and thermal-expansion measurements on the quasi-two-dimensional $S=1/2$ honeycomb-lattice compound $InCu_{2/3}V_{1/3}O_3$. These experiments were carried out to establish the crystal structure, and, in particular, the previously proposed Cu-V ordering and the layer stacking.[9] Another important aspect is the question of antiferromagnetic long-range order (LRO). In an earlier publication, the onset of three-dimensional (3D)-LRO below $T=38$ K was tentatively proposed from magnetization data, displaying a kink in $\chi(T)$ and a vanishing electron spin resonance (ESR) signal.[9] However, we will show below that the kink in $\chi(T)$ is more likely due to a domain boundary effect. The susceptibility shows a very broad maximum around 150 K, indicative of low-dimensional magnetic correlations. It is interesting to note that there are various examples of $A_nCu_{n-1}BO_{3n}$ compounds. For $n=4$ antiferromagnetic $La_4Cu_3MoO_{12}$ was reported to exhibit a kagomé-like lattice consisting of triangular clusters of copper $S=1/2$ ions[10–12] and for $n=3$, apart from the title compound, $La_3Cu_2VO_9$ also has been synthesized. In this latter paramagnetic compound, the copper and vanadium ions are believed to order in a superstructure with Cu_3O clusters.[13] For $n=2$ several compounds have been reported with three different possibilities for Cu-B cation arrangements.[14] With these structural considerations in mind, it seemed worthwhile to elucidate the proposed Cu-V arrangement in our $n=3$ compound by neutron and x-ray diffraction, as well as spectroscopic investigations to probe the local structural features. Once the structure has been determined, we employ thermodynamic methods to test the magnetic properties. Finally, quantum-Monte Carlo (QMC) calculations were performed to confirm the two-dimensional (2D) magnetic correlations.

II. EXPERIMENT

$InCu_{2/3}V_{1/3}O_3$ was synthesized from the oxides by a conventional solid-state technique. In_2O_3, CuO, and V_2O_5 in a molar ratio of 3:4:1 were thoroughly ground and pressed into pellets. These were then heated at 1173 K in air for five days, slowly cooled, reground, pressed into pellets, and heated again for two days. Sample purity was checked by powder x-ray diffraction, which showed no impurity peaks. Further confirmation was obtained from synchrotron data (not shown here) measured at Delta, Dortmund. Details of the experimental setup are given in Ref. 15. High-resolution measurements of the linear thermal-expansion coefficient $\alpha=1/L\cdot\partial L/\partial T$ (L is the length of the sample) have been performed in the temperature range from 4 to 180 K using a home-built capacitance dilatometer.[16] Specific-heat measure-

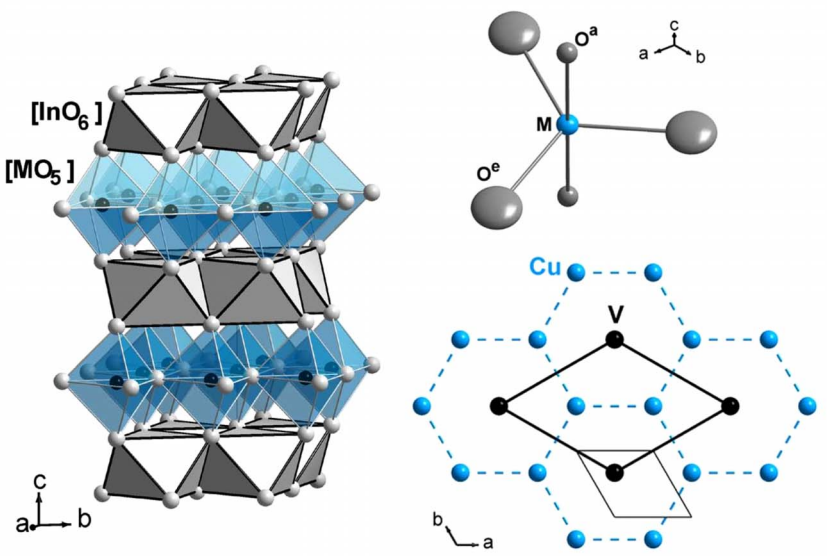

FIG. 1. (Color online) Perspective view of the crystal structure of $InCu_{2/3}V_{1/3}O_3$ with $[InO_6]$ and $[MO_5]$ polyhedra (left). On the right (top), a $[MO_5]$ entity is shown with the thermal ellipsoids given with 75% probability [single-crystal data at 293 K (Ref. 18)]. Below the in-plane Cu/V order representing the honeycomb structure (dashed lines) without the oxygen atoms is given with the respective unit cell for $P6_3/mmc$ (reference axis, line) and $p31m$ (bold line). Note that there are two distinct crystallographic sites for copper and vanadium. The lattice parameters are $a_{p31m}=\sqrt{3}a_{P6_3/mmc}\approx 5.8$ Å.

ments were carried out from 25 K to room temperature using a home-built calorimeter working with a quasiadiabatic continuous-heating method and with a nonadiabatic method (PPMS system, Quantum Design) from 1.8 to 300 K.

The temperature dependence of the lattice parameters has been determined on a Siemens *D*-5000 diffractometer with a ^{4}He-flow cryostat using Cu-K_α radiation. Lattice parameters were determined from a LeBail fitting routine. Powder neutron-diffraction experiments were performed at the Orpheé-reactor in Saclay, Laboratoire Léon Brillouin (LLB), on the high-resolution diffractometer 3T.2 ($\lambda\approx 1.2$ Å; instrument parameters: $u=0.257923$, $v=-0.392569$, and $w=0.200459$) and the high-flux diffractometer G4.1 ($\lambda\approx 2.4$ Å; instrument parameters: $u=0.8210$, $v=-0.2370$, and $w=0.0780$). Two samples of approximately 6 g from two different batches were filled into vanadium containers of 6 mm radius. Rietveld analysis was carried out using the program FULLPROF.[17] Mid-infrared (MIR) and far-infrared data (FIR) of $InCu_{2/3}V_{1/3}O_3$ were collected at room temperature using standard KBr and polyethylene (PE) disk techniques, respectively, on a Bruker FTIR 66 s/v spectrometer. Spectra in the visible (Vis) and near-infrared (NIR) regions were recorded on a Cary 05E spectrometer (Varian) at room temperature.

III. CRYSTAL STRUCTURE

$InCu_{2/3}V_{1/3}O_3$ was previously reported to crystallize in the hexagonal space-group $P6_3/mmc$ (single-crystal x-ray data), consisting of alternating layers of $[InO_6]$ octahedra, and Cu^{2+} and V^{5+} ions in a trigonal-bipyramidal coordination[9] (see Fig. 1). The Cu^{2+} ions are proposed to be arranged on a honeycomb lattice with the nonmagnetic V^{5+} ions in the center, as sketched in the bottom right-hand side of Fig. 1. All x-ray and neutron-diffraction measurements can be described quite well within the structural model in space-group $P6_3/mmc$, derived from the $YAlO_3$ (Ref. 19) type of structure, which is also observed for the high-temperature modification of $InMnO_3$ (see Fig. 2). In this structure type the $[InO_6]$ polyhedra are linked via edges to layers in (001) and are separated by layers of corner sharing $[MO_5]$ units ($M=2/3$ Cu and 1/3 V). It is interesting to note that for $M=$Mn, a triangular lattice of paramagnetic ions is present, giving rise to frustration phenomena. A structural phase transition to the low-temperature modification ($P6_3cm$) occurs in $YMnO_3$.[20,21] This transition is related to buckling of the Mn/O-layers. In contrast, for $InCu_{2/3}V_{1/3}O_3$ no signs of structural changes down to 1.5 K have been observed. Indeed, no frustration is expected for an arrangement of the magnetic Cu ions on a honeycomb type of structure.

Since in this structural model ($P6_3/mmc$), the Cu^{2+} and V^{5+} ions occupy the same crystallographic site statistically in a two to one ratio; this allows, in principle, the formation of a honeycomb lattice for these ions, as shown in Fig. 1. Furthermore, this structural Cu^{2+}/V^{5+} order will imply superstructure reflections in any diffraction experiment, which, however, cannot be observed by x-ray diffraction due to the little contrast of Cu and V. The crystallographic data of the averaged model ($P6_3/mmc$) obtained by powder neutron scattering on the 3T.2 diffractometer at room temperature and $T=10$ K are summarized in Table I, with the patterns shown in Fig. 2. Furthermore, averaged (Cu/V) to oxygen distances occur, which are in contrast with the local structure expected for the different transition-metal cations. Spectroscopic data give evidence for the two local environments of the $[CuO_5]$ and $[VO_5]$ polyhedra, respectively.

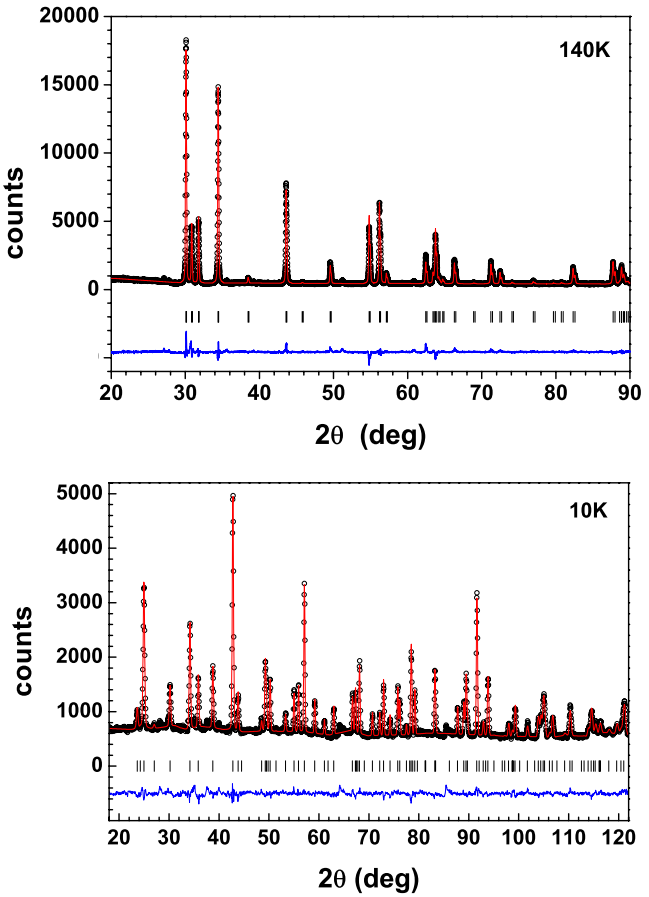

FIG. 2. (Color online) Typical Rietveld refinement of powder x-ray diffraction data at 140 K (above) and neutron-diffraction data measured on the 3T.2 beamline (LLB) at 10 K. Refinements were carried out in the average structure model in space-group $P6_3/mmc$ (see Table I).

IV. INFRARED SPECTROSCOPY

In a first attempt we analyze our infrared phonon data in a molecular approach. There are five normal modes to be expected in the IR region for a $[MO_5]$-complex (D_{3h}). These are of A_2'' [$\nu_3 \equiv \nu_{as}$(M-O^a) and $\nu_4 \equiv \gamma$(M-O^e)] and E' [$\nu_5 \equiv \nu_{as}$(M-O^e), $\nu_6 \equiv \delta$(M-O^e), and $\nu_7 \equiv \delta$(M-O^a)] symmetries.[22,23] Since Cu^{2+} and V^{5+} differ by charge and interatomic distances d(M-O), there are two sets of five normal modes to be expected. Figure 3 gives a comparison with lattice-dynamical calculations for $YMnO_3$ (space-group $P6_3/mmc$) for a $[MnO_5]$ complex.[24] Independent of the respective cation ($M = V^{5+}$, Mn^{3+}, and Cu^{2+}), the relative frequency change within one set for each central cation is approximately the same. A splitting of the asymmetric stretching frequencies is present for the axial and equatorial metal to oxygen modes, which is a measure for different force constants reflecting differences in bonding interaction. Separations in the frequency of each normal mode occur for different cations, e.g., $\nu_3(V^{5+}) > \nu_3(Mn^{3+}) > \nu_3(Cu^{2+})$.

In $InCu_{2/3}V_{1/3}O_3$ one may roughly distinguish regions of different phonon character. In general the character of the modes follows the masses with the highest modes being of O bond-stretching character. The lowest modes can be associated with In vibrations, and the splitting of modes due to Cu/V mixing induces a separation of Cu-related modes ($\lesssim$400 cm^{-1}) and V-related modes ($\gtrsim$400 cm^{-1}). The measured frequencies clearly document that the high-temperature value of $c_p \sim c_v$ of $5(3R) = 124.7$ J/(mol K) at 300 K will

TABLE I. Positional parameters for $InCu_{2/3}V_{1/3}O_3$ at different temperatures, as determined by NPD (3T.2 instrument). All refinements were carried out in space-group $P6_3/mmc$ in which in Wyckoff notation indium is on the ($2a$) site (0 0 0), copper and vanadium are distributed on the ($2c$) site ($\frac{1}{3}$ $\frac{2}{3}$ $\frac{1}{4}$), O^e is on ($2b$) (0 0 $\frac{1}{4}$), and O^a is on the fourfold ($4f$) position ($\frac{1}{3}$ $\frac{2}{3}$ z) with a refineable z position. Refined parameters during Rietveld refinement are the lattice parameters and atomic position of O^a, and overall temperature factor, peak shape, preferred orientation, and asymmetry parameters as well as parameters for the sample geometry.

	NPD	NPD
T (K)	300 K	10 K
χ^2	4.02	3.81
R_{Bragg}	7.91	6.56
RF factor	7.39	6.72
a (Å)	3.3571(3)	3.3509(4)
c (Å)	11.9165(2)	11.9012(4)
O^a z parameter	0.0863(2)	0.0864(3)
B_{iso} (Å^2):		
In ($2a$)	1.02(4)	0.94(3)
(Cu/V) ($2c$)	1.20(4)	1.03(3)
O^a ($4f$)	1.04(3)	1.06(2)
O^e ($2b$)	2.57(5)	2.56(6)
Interatomic distances (Å):		
(Cu/V)-O^a	1.951(5)	1.947(3)
(Cu/V)-O^e	1.938(4)	1.935(4)
$(Cu\text{-}Cu)_{in\text{-}plane}$	3.357(2)	3.351(3)
In-O	2.194(2)	2.191(3)

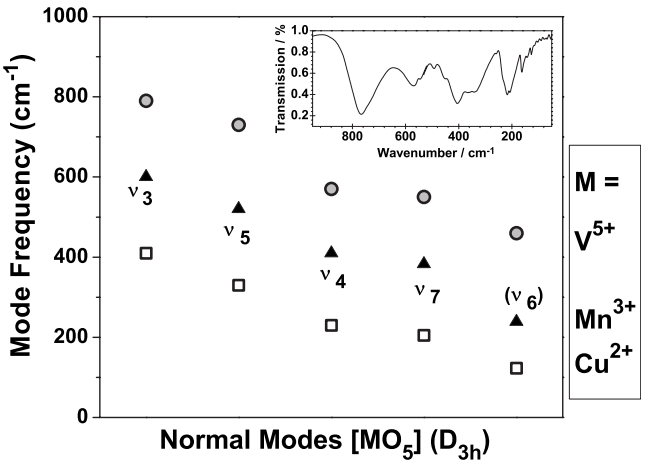

FIG. 3. Comparison of calculated normal modes for $[MnO_5]$ (triangles, taken from Ref. 24) and observed normal modes for $InCu_{2/3}V_{1/3}O_3$ (circles and squares). The assignment given in brackets is tentative. The measured infrared spectrum is shown in the inset.

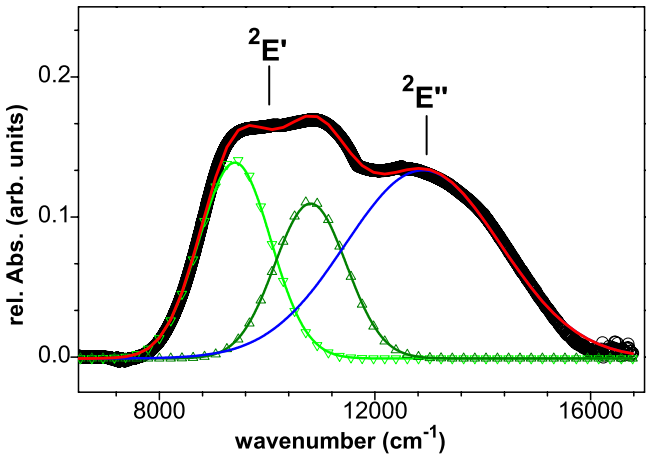

FIG. 4. (Color online) Electronic spectrum of $InCu_{2/3}V_{1/3}O_3$ showing the two principal transitions. A Gaussian fit is given for the two members of the $^2E'$ (green triangles) and the $^2E''$ transition (blue line) as well as the sum displayed in red.

still be reduced by more than $1/3(3R)=R$, which corresponds well with the extrapolated value of the specific heat of ~110 J/(mol K).

Calculated lattice contributions (phonons) to the specific heat for $REMnO_3$ (RE=Y,Lu,Sc) in respect to the "heavy" (Mn, RE) and "light" (O) elements, with Θ_D^{heavy} =350–420 K and Θ_D^{light}=780–800 K, have been used by Tomuta *et al.*[25] These are related to the normal modes (Fig. 3) of 325 K~225 cm^{-1} for the lowest Mn-O vibration and of 600 cm^{-1}~860 K for the upper limit. In the case of $InCu_{2/3}V_{1/3}O_3$ this would suggest three regions for the activation of In-O, Cu-O, and V-O vibrations, and all normal modes, ~160, 350, and 710 K. We will use these as Einstein modes to account for the lattice contributions (phonons) to the specific heat (see below).

V. VISIBLE-NEAR-INFRARED SPECTROSCOPY

The observed absorption spectrum for $InCu_{2/3}V_{1/3}O_3$ is shown in Fig. 4, and consists of two principal bands (≈9800 and ≈12900 cm^{-1}) related to the $^2A_1'$ to $^2E'$ and $^2E''$ transitions for a chromophore of D_{3h} symmetry (Cu^{2+}, d^9), respectively. The *d*-orbital splitting corresponds to d_{z^2} $(a_1')>d_{xy}$, $d_{x^2-y^2}$ $(e')>d_{xz}$, and d_{yz} (e'') in this case. If the true symmetry of $[CuO_5]$ would be D_{3h} symmetry, the $E_2(^2A_1\rightarrow{}^2E'')$ transition should be forbidden. Instead rather similar intensities are observed for E_1 and E_2, which might have different origins, e.g., vibronic coupling or reduced symmetry. According to the angular-overlap model (AOM) (Refs. 26 and 27), the relative energies can be related to σ- and π-antibonding interactions between the oxygen ligands and the metal cation according to

$$E(z^2)=2e_\sigma^a+\tfrac{3}{4}e_\sigma^e-e_{ds},$$

$$E(x^2-y^2,xy)=\tfrac{9}{8}e_\sigma^e+\tfrac{3}{2}e_\pi^e,$$

$$E(xz,yz)=2e_\pi^a+\tfrac{3}{2}e_\pi^e. \quad (1)$$

Since the equatorial (*e*) and axial (*a*) interactions may be different due to differences in the interatomic Cu-O distances, and/or connectivities to nonequivalent chemical elements (e.g., Cu-O^a-In and Cu-O^e-V), a global parameter e_{ds} referring to *d-s* mixing should be included (see also Ref. 27). This will lead to a substantial lowering of the d_{z^2} orbital. If we take the energy difference E_2-E_1 without an e_{ds} contribution, and equal equatorial and axial interaction parameters, the e_σ/e_π ratio is approximately 3.5:1 and e_σ~8000 cm^{-1}.

The first question that needs to be addressed here is how the $[CuO_5]$ unit distorts. The two possible scenarios are an elongated or a compressed geometry. Starting from $d(\text{Cu-O}^{e,a})=1.94$ Å with e_σ~8000 cm^{-1} and $e_\pi\sim e_\sigma/3.5$, the two distortions are simulated by reducing the respective axial and equatorial interactions proportional to a d^{-5} law. Best fits to the observed spectra were found for the compressed geometry with $e_\sigma^e\sim e_\sigma^a/1.176$ without e_{ds} mixing, which implies $d(\text{Cu-O}^e)$ ~2.01 Å$>d(\text{Cu-O}^a)\sim1.94$ Å. This is consistent with the observation of rather large displacement factors of the equatorial oxygen sites in the hexagonal plane [$U_{11}(O^e)\sim6$ $U_{11}(O^a)$ from single-crystal data and for B_{iso} of the powder refinements, see Table I]. Furthermore this reflects the expected differences of d(V-O^e) and d(Cu-O^e). For d(V-O^e), values of ~1.8 Å can be anticipated due to the higher oxidation state of V^{5+} compared to Cu^{2+} (see also the IR data above), in agreement with the observed average distance for d[(V/Cu)-O^e] of ~1.94 Å.

The introduction of the global e_{ds} parameter of 880 cm^{-1}, according to the differences in e_σ^e and e_σ^a, yields $E_1(^2A_1'\rightarrow{}^2E')\sim9770$ cm^{-1} and $E_2(^2A_1'\rightarrow{}^2E'')\sim12900$ cm^{-1}, and is in good agreement with the observed electronic spectrum.

If we take the observed *g* value of 2.24 into account,[9] we can estimate the orbital reduction factor $k_\perp\sim0.81$ from Eq. (2), neglecting third order contributions,

$$g_\perp=g_0+6u_\perp-6u_\perp^2;\quad u_\perp=k_\perp^2\frac{|\lambda_0|}{E_2}, \quad (2)$$

with λ_0=830 cm^{-1} and g_0=2.00. The absorption spectrum further reveals a splitting of the $E_1(^2A_1'\rightarrow{}^2E')$ transition of ~1400 cm^{-1} due to spin-orbit coupling, which is related to the energy difference by $\Delta=2k\lambda_0\sim1350$ cm^{-1} with k =0.81. The expected spin-orbit splitting of the $E_2(^2A_1'\rightarrow{}^2E'')$ transition is approximately 500 cm^{-1} and not resolved in the spectrum. The results obtained from the ligand-field approach for the $[CuO_5]$ unit are: (i) The complex should be a compressed trigonal bipyramid [d(Cu-O^a) $<d$(Cu-O^e)] with slight deviations of the equatorial O^e-Cu-O^e angles of less than ±3° from 120°. (ii) The derived orbital reduction factor k is in good agreement with other oxocuprates(II).[28] (iii) Both ESR (Ref. 9) and these spectroscopic investigations show the important contribution of spin-orbit coupling and e_{ds} mixing for this geometry.

VI. NEUTRON POWDER DIFFRACTION AND DOMAIN STRUCTURE

Our objective for carrying out the neutron-scattering experiment on $InCu_{2/3}V_{1/3}O_3$ was to find evidence of the as-

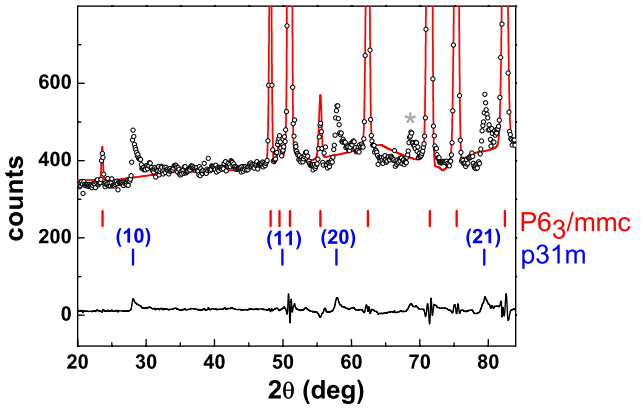

FIG. 5. (Color online) Neutron powder-diffraction pattern of $InCu_{2/3}V_{1/3}O_3$ at 1.5 K measured on instrument G4.1 (LLB). Superstructure reflections can be seen at $2\theta \approx 28°$, 50° (overlapping with a 3D Bragg peak), 58°, and 79.5°. These are marked with 2D Miller indices (10), (11), (20), and (21) according to the model shown in Fig. 1 and Table II. The peak marked by an asterisk originates from the sample holder.

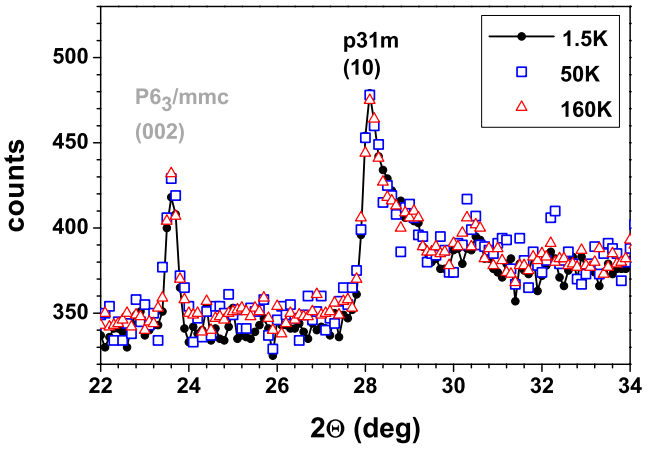

FIG. 6. (Color online) Neutron powder-diffraction patterns of $InCu_{2/3}V_{1/3}O_3$ measured on instrument G4.1 (LLB). For the (002) and the (10) reflection data are shown for 1.5, 50, and 160 K, indicating the temperature independent nature of the 2D superstructure reflections.

sumed honeycomblike Cu/V order. The difference in scattering factors for copper and vanadium is much larger for neutrons than for x-rays so that the intensity of superstructure reflections should be enhanced. As V is a very weak and Cu a strong scatterer in the case of neutron diffraction, one expects super-lattice intensities of the order of 5%–10% of a fundamental Bragg peak. A close inspection of the diffraction pattern measured at 10 K on the high-resolution LLB instrument 3T.2 shown in Fig. 2 reveals the presence of four asymmetric peaks that are not indexable in $P6_3/mmc$. These exhibit typical 2D scattering Warren line shapes that can be observed far better in the measurements performed on the high-flux instrument G4.1 (see Fig. 5). All four reflections can be indexed in the 2D space-group $p31m$ with $a_{p31m} = \sqrt{3}a_{P6_3/mmc} \approx 5.8$ Å, assuming the in-plane structural model shown in Fig. 1, and confirming the previously assumed honeycomblike arrangement of the copper ions. In this model, the Cu and V ions occupy two distinct crystallographic sites (see Table II and Ref. 29).

Warren showed that the full widths at half maximum (FWHM) of the asymmetric reflections are a direct measure for the structural correlation length L_0, which indicates the size of crystallographically ordered domains within a quasi-2D structure.[30] The intensity distribution of a 2D Bragg reflection takes the form

TABLE II. Positional parameters of the copper and vanadium ions of the structural model in the 2D space-group $p31m$. The lattice constant a_{p31m}=5.8048(3)Å is obtained by a two-phase Rietveld refinement of the G4.1 measurement at 1.5 K.

	Wyckoff	x	y
Cu	2b	2/3	1/3
V	1a	0	0

$$I(2\theta) = \mathrm{Km}\frac{F_{hk}^2(1+\cos^2 2\theta)}{2(\sin\theta)^{3/2}}\left(\frac{L_0}{\sqrt{\pi}\lambda}\right)^{1/2} F(a), \qquad (3)$$

where K is a constant, m the multiplicity, F_{hk} a two-dimensional structure factor, and λ the wavelength. The function $F(a)$ is tabulated.[30] Using this expression, we have extracted the structural in-plane correlation length L_0 and found a constant value of approximately 300 Å independent of temperature (see Fig. 6). The intensities of these 2D reflections also remain constant for the measured temperatures at 1.5, 50, 160, and 220 K. A Warren-type fit to the (10) and (20) peaks is shown in Fig. 7. We note that even at 300 K the intensities do not exhibit any significant change, as can be seen in the 3T.2 measurements that were performed at 10, 150, and 300 K. Therefore, these asymmetric peaks are of

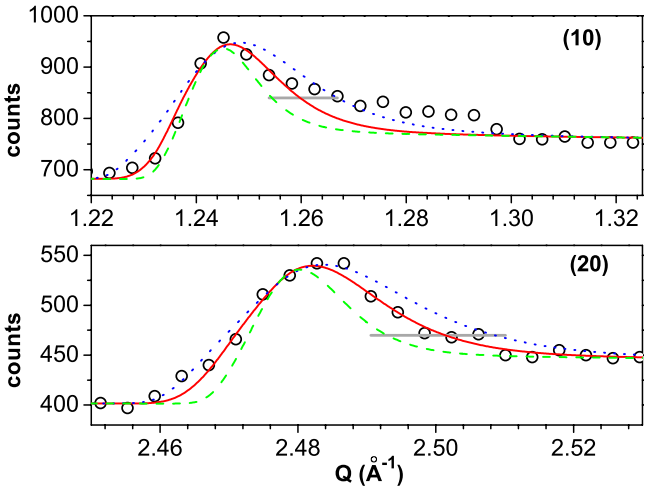

FIG. 7. (Color online) Warren line shape fits to the data using Eq. (3) for the 2D superstructure reflections (10) and (20) at 1.5 K with L_0=250 Å (blue dotted line), L_0=300 Å (red line), and L_0 =500 Å (green dashed line). The instrumental resolution of the G4.1 instrument is indicated by the gray horizontal lines.

structural origin and are not associated to magnetic 3D-LRO. Due to its two-dimensional nature, it is not obvious to estimate the absolute scale of the Cu-V ordering. A three-dimensional stacking of honeycomb ordered planes can be described in the space-group *Cmcm* with lattice constants 10.3, 5.8, and 11.3 Å. In this model neighboring planes are ordering in phase. This model allows direct comparison of the integrated intensity in the 2D-Warren-shape superstructure reflections with the fundamental Bragg reflections. It appears that the observed intensity is somehow weaker than the prediction by the model of perfect Cu/V order but any precise analysis is prohibited by the impossibility to separate the tails of the Warren-shape functions from the background.

Apart from confirming the proposed 2D Cu-V ordering in domains ($p31m$), the asymmetry of the superstructure reflections indicates a random arrangement of the [(Cu/V)-O^e] planes along the c axis. This is consistent with the averaged structure ($P6_3/mmc$) observed by x-ray diffraction techniques. The refinement of the structure model in space-group $P6_3/mmc$ fully ignores the local displacements induced by the Cu/V order. Although there is no long-range three-dimensional order, these displacements will induce atomic displacement parameters (ADPs) much larger than normal thermal parameters arising from thermal movements (Debye-Waller parameters). We have described the ADPs by isotropic factors, B_{iso}, which are nearly temperature independent in agreement with the fact that the Cu/V order as well as the induced displacements are temperature independent below room temperature. The remarkably large $B_{\mathrm{iso}} \sim 1-2$ Å^2 values fitted for all sites indicate large root-mean-square displacements of the order of ~0.1 Å, in perfect agreement with the strong differences in the ionic radii (~0.15 Å) mentioned above.

VII. LATTICE AND THERMAL EXPANSIONS, AND SPECIFIC HEAT

To extract the low-temperature thermal evolution of the lattice parameters, x-ray diffraction patterns were refined in the space-group $P6_3/mmc$ by profile matching (see also Fig. 2). No signs of a structural phase transition were observed in the temperature range from 25 to 300 K. The temperature dependence of the lattice parameters is shown in Fig. 8. As expected, the cell volume decreases linearly toward lower temperatures until it reaches a plateau at around 100 K. A rather large anisotropy can be detected by comparing the temperature dependence of the a and c axes. While c reaches a plateau already at roughly 150 K, the a axis decreases smoothly with decreasing temperature and approaches a finite value below 100 K. The thermal-expansion coefficients differ significantly with $\alpha_c \approx 2.65 \cdot 10^{-6}$ K^{-1} and $\alpha_a \approx 8.43 \cdot 10^{-6}$ K^{-1} above 200 K. There is even evidence that the thermal-expansion coefficient along c is negative at low temperature, as it is frequently observed in systems with soft buckling modes of rigid units.

In Fig. 9 the result of the linear thermal-expansion measurement $1/L \cdot \partial L/\partial T$ of a pressed and then sintered powder sample is given in comparison with the derived temperature dependence of $\alpha_a = 1/a \cdot \partial a/\partial T$, $\alpha_c = 1/c \cdot \partial c/\partial T$, and $\alpha_{\mathrm{V}} = 1/(3\ \mathrm{V}) \cdot \partial \mathrm{V}/\partial T$ from the x-ray diffraction data ($P6_3/mmc$). Due to the pronounced structural anisotropy, the c direction contributes only 17% to α_{V} at room temperature and almost nothing at low temperatures. The measurement of the specific heat $c_p(T)$ is also included in Fig. 9; it roughly scales with the thermal-expansion coefficients. In the following, we may neglect the difference between c_p and c_v due to the very small thermal expansion below room temperature. With the capacitance dilatometer, we, furthermore, obtain

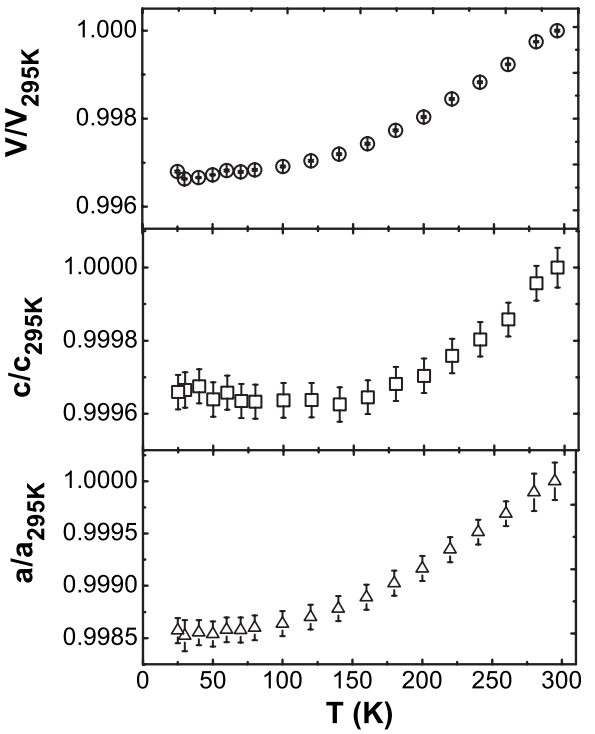

FIG. 8. Normalized temperature dependence of the lattice parameters and the cell volume of $InCu_{2/3}V_{1/3}O_3$ obtained by temperature-dependent x-ray powder diffraction.

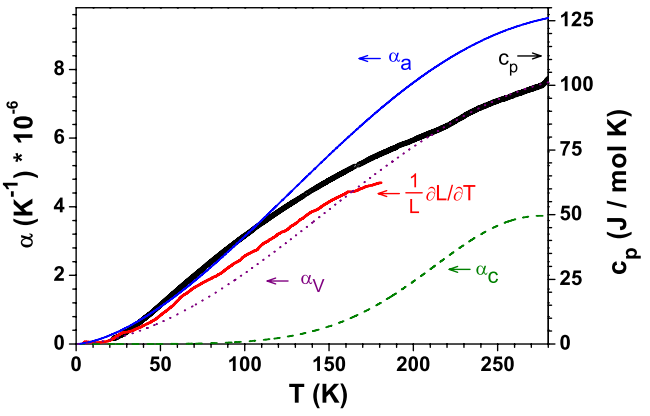

FIG. 9. (Color online) The temperature dependence of the thermal-expansion coefficients for $InCu_{2/3}V_{1/3}O_3$ determined from the x-ray diffraction data: α_a (blue), α_c (green, dashed), and α_{V} (violet, dotted) in comparison with the thermal-expansion measurement $1/L \cdot \partial L/\partial T$ (red) are shown (left axis). The experimental specific-heat data, $c_p(T)$ (black circles, home-built calorimeter data), are included as well (right axis).

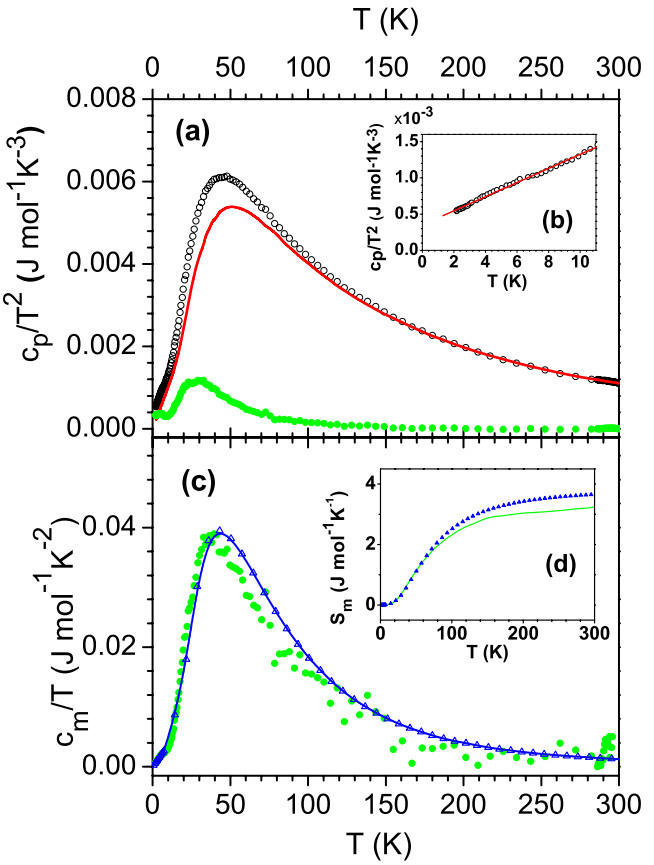

FIG. 10. (Color online) The temperature dependence of the measured specific heat divided by T^2 (black circles, PPMS data) of $InCu_{2/3}V_{1/3}O_3$ is shown in (a). The red line indicates the calculated phononic contribution applied to extract the magnetic specific heat, c_m/T^2 (green circles). Inset (b): the low-temperature regime of the specific heat divided by T^2 (circles) and the applied linear fit (red line) is depicted. In (c) the calculated magnetic part of the specific heat divided by T (c_m/T) obtained from QMC methods (blue triangles) is compared with the phonon corrected experimental data (circles). (Note that $c_m \propto AT^2$ cannot be discerned from this plot, see also Ref. 31.) The magnetic part of the entropy is plotted in inset (d) for the phonon corrected experimental data (line) and the results of QMC calculations (blue triangles).

$1/L \cdot \partial L/\partial T$ with a very high relative precision; this experiment is thus very sensitive in detecting structural or magnetic phase transitions. However, neither $1/L \cdot \partial L/\partial T$ nor the $c_p(T)$ data in Fig. 9 yield any evidence for such a transition.

The measured c_p/T^2 data versus temperature are given in Fig. 10(a). No indication of a 3D long-range order is observed in this temperature region, especially around 38 K where conventional magnetic order seems to be absent. The specific heat of low-dimensional spin systems is notoriously difficult to calculate and to compare with experiments that are dominated by phonon contributions. It is fair to say that for a few one- or two-dimensional Heisenberg systems with an exchange integral larger than a few Kelvin, the full specific heat at all temperatures has not been successfully and reliably calculated and compared with experimental data (see, e.g., Ref. 32). Although these limitations also hold for $InCu_{2/3}V_{1/3}O_3$, we fortunately have obtained very reliable low-temperature measurements of the specific heat, which allow an extraction of the magnetic contribution at $T < 20$ K. The behavior of the specific heat in this temperature range is well described by a T^3 law originating from the (Debye) phonons and a T^2 term from the 2D magnetic contribution,

$$c_m(T) = 0.597R\left(\frac{T}{J}\right)^2, \tag{4}$$

where the prefactor 0.597 originates from a fit,

$$U_m(T) = 0.199\left(\frac{T}{J}\right)^3, \tag{5}$$

of the internal energy, as obtained by QMC (see also Ref. 31 for further details).

A linear fit $y = A + BT$ to the measured specific-heat data divided by the squared temperature (c_p/T^2) below 12 K yields $A = 0.00034 \frac{J}{\text{mol K}^3}$ and $B = 0.00010 \frac{J}{\text{mol K}^4}$ [see Fig. 10(b)]. If we insert $J_{AF} = 120$ K into Eq. (4), we obtain the prefactor $A = 0.00035 \frac{J}{\text{mol K}^3}$, representing the magnetic contribution to the total specific heat calculated by QMC in excellent agreement with the fit to the experimental data. It should be noted that for $J_{AF} = 140$ K, which is the value of the exchange interaction previously obtained from a fit to the magnetic-susceptibility data,[9] we find a slightly smaller value of $A = 0.00026 \frac{J}{\text{mol K}^3}$.

In the low-temperature region, we used the Debye model,

$$\lim_{T \to 0} c_{\text{phon}}(T) = 233.8R\left(\frac{T}{\Theta_D}\right)^3, \tag{6}$$

to calculate the linear dependence of c_p/T^2. With $B = 0.00010 \frac{J}{\text{mol K}^4}$ we obtained a value of $\Theta_D = 268$ K in this temperature region. The inset [panel (b)] of Fig. 10 displays the linear fit of the c_p/T^2 data at temperatures below 12 K.

Based upon the ranges of vibrational modes discussed in Sec. IV, we obtain three characteristic mode temperatures whose values are ≈160, 350, and 710 K, (see also Ref. 33 for further details). If we insert these values as Einstein modes into the Einstein formula for the specific heat,

$$c_{\text{phon}}(T) = \frac{3R\left(\frac{\Theta_E}{T}\right)^3 e^{\Theta_E/T}}{(e^{\Theta_E/T} - 1)^2}, \tag{7}$$

we achieve a good fit to the measured c_p/T^2 data in the high-temperature range above 150 K, as shown in Fig. 10(a). The deviations below ≈150 K represent the magnetic contributions c_m/T^2. After subtracting the phonon contributions for the whole measured temperature range (details given in Ref. 33), the magnetic part c_m is obtained and compared with the results from QMC calculations for $J_{AF} = 120$ K in Fig. 10(c). These results are in reasonable agreement with the phonon corrected measurement. This is further illustrated in the inset [panel (d)] where the derived entropy (S_m) is plotted versus temperature. For $InCu_{2/3}V_{1/3}O_3$ a value of $\frac{2}{3}R \ln 2 = 3.84 \frac{J}{\text{mol K}}$ is expected. The slightly smaller experimental value of $3.4 \frac{J}{\text{mol K}}$ resulted due to inaccuracies in the phonon correction.

The calculated magnetic contribution to the specific heat from QMC methods for the honeycomb lattice with $J_{AF}=120$ K indicates that a large fraction of the magnetic entropy is connected with short-range correlations below ≈ 100 K. From Fig. 9 in this temperature region, the (structural based) thermal expansion α_a is mainly temperature dependent whereas α_c is almost constant and very small, which also indicates the dominant 2D character.

To summarize the above results, we found no evidence for a 3D Néel-type transition at ≈ 38 K, as suggested in Ref. 9. There are various mechanisms that could produce a kink in the susceptibility without long-range order, such as local domain boundaries (see below). Identifying this feature with a Néel transition at a temperature where the system orders 3D magnetically is problematic because we do not see any 3D magnetic peaks in the neutron-scattering data and there is no indication of a phase transition in the specific heat. The sensitivity of the neutron-diffraction experiment to weak magnetic order is however strongly reduced due to the 2D character of the Cu-V structural ordering. A magnetic order with an ordered moment of about half a μ_B on the Cu sites would imply a magnetic intensity about 30 times smaller than that arising from nuclear scattering on copper and vanadium. Furthermore, the stacking of planes with the 2D feature of the honeycomb structure type is not regular, i.e., the planes are shifted with respect to each other along [001], which prohibits the formation of a well defined translation symmetry. Therefore, we believe that we can exclude the possibility of a 3D Néel order as origin of the susceptibility anomaly at low temperature.

VIII. SPIN CORRELATION LENGTH AND FINITE-SIZE EFFECTS

The finite temperature properties of the Heisenberg antiferromagnet on a honeycomb lattice were evaluated theoretically by a continuous time quantum-Monte Carlo (QMC) algorithm.[34] This method allows us to study both the magnetic part of the specific heat $c_m(T)$ and the correlation length $\xi(T)$ down to low temperatures. While the computation of the specific heat is fairly straightforward, we now make a few comments on the calculation of the correlation length: From earlier works,[35,36] one expects the honeycomb lattice to show magnetic Néel order similar to the two-dimensional square lattice Heisenberg antiferromagnet at $T=0$. In order to corroborate this picture, we calculated the spin-spin-correlation function for various system sizes and extracted $\xi(T)$ by explicitly fitting a periodically symmetrized Ornstein-Zernike formula to the data. To obtain a reliable value for the correlation length, we choose the system sizes approximately four times larger than the expected correlation length in order to keep finite-size effects small. (see, e.g., Ref. 37). From our analysis, we infer that the correlation length diverges exponentially as the system approaches zero temperature. This is shown in Fig. 11 for a system of 256×512 spins and it means that the honeycomb lattice displays a similar behavior as the square lattice but with the spin stiffness D_{HC} significantly reduced compared to the square lattice. As explained above, the experimental results suggest

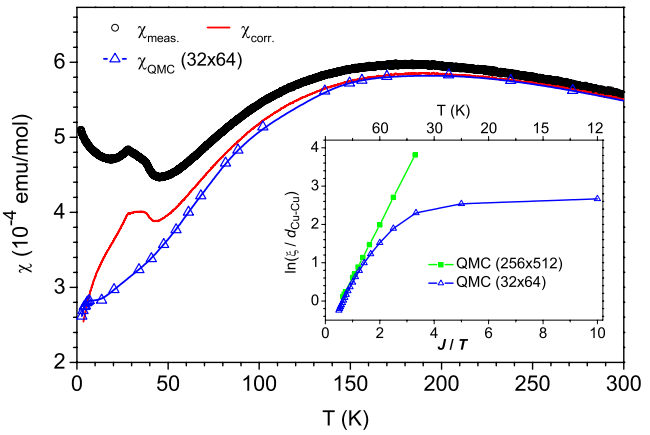

FIG. 11. (Color online) Main panel: Susceptibility as measured ($\chi_{meas}(T)$, circles), correction for paramagnetic impurities at defect sites ($\chi_{meas}(T)$-$\chi_{CW}(T)=\chi_{corr}(T)$, red line), and the calculated susceptibility from QMC methods for $J_{AF}=120$ K (triangles, blue). A logarithmic plot of the spin-spin-correlation length in units of shortest Cu-Cu contacts from QMC calculations for two different systems is shown in the inset. Note that $\xi(T)$ diverges above $J/T=1$, e.g., below 120 K and approaches a finite value below ≈ 50 K, according to QMC calculations for a system of 32×64 spins.

the 2D structural correlation length of $L_0 \sim 300$ Å ($\approx 90 \times 90$ spins), where structural order of a honeycomb lattice exists to be the upper limit of the magnetic correlation. We therefore also calculated the correlation length for finite lattices. Figure 11 shows the results for a system with 32×64 spins. In this case $\xi(T)$ approaches a constant value as T approaches zero. (Clearly it cannot exceed the size of the magnetic domains). These data obtained from QMC calculations coincide well above 120 K with the magnetic-susceptibility data corrected for impurities due to uncompensated spins at defect sites. These have been estimated from the low-temperature upturn ("tail") in the susceptibility to be less than 1%, assuming a Θ_{CW} value of 10 K (see also Ref. 9). Below 120 K the corrected experimental susceptibility and the $\chi_{QMC}(T)$ data for 32×64 spins differ slightly. This can be understood in terms of the above discussed spin-spin-correlation length (see the inset of Fig. 11). Noteworthy is the temperature region below ≈ 50 K with $\xi(T)$ approaching a constant value. Therefore, we tentatively ascribe the kinks in the low-temperature regime $T \approx 30$ K and $T \approx 38$ K to local magnetic correlations of unsaturated spins at the structural domain boundaries. These unsaturated spins most probably freeze into a glassylike state, which is detected as kinks in the susceptibility (see also Ref. 38). The field dependence of these features (not shown here) support this interpretation and further dynamical measurements are in progress.

IX. CONCLUSIONS

We presented results on the local structure of the $[MO_5]$ units with $M=Cu^{2+}$ and V^{5+} derived from IR spectroscopy, which also gave detailed insight into the electronic structure of the $[CuO_5]$ chromophore. As it is expected from Pauling's rules, the exclusive connectivity of V-centered polyhedra

with $[CuO_5]$ units is favored within the layers due to the large differences in charge of the transition-metal cations, effectively minimizing the repulsive interaction. Thereby, the formation of a honeycomb lattice for the magnetic Cu ions results as the most likely scenario of cation ordering for the statistical occupation of a common site ($P6_3/mmc$). The intriguing question why this Cu/V order is not directly observed in x-ray powder-diffraction experiments and subsequently gives rise to a 3D superstructure is solved here. NPD data clearly indicate that this structural order only persists in 2D domains of ~300 Å size, which is some order of magnitude lower than the grain size of the particles. No stacking order along the *c* direction can be observed. The magnetic data and the magnetic contribution to the specific heat can be described theoretically by application of quantum-Monte Carlo methods. In particular finite-size effects, which are observed in the susceptibility below 50 K due to the domain structure present in $InCu_{2/3}V_{1/3}O_3$ may be understood in terms of our QMC results obtained for the spin-spin-correlation length.

ACKNOWLEDGMENTS

Support by the Deutsche Forschungsgemeinschaft (SFB 608) and funding through the European Commission "6th Framework Program, NMI3" is gratefully acknowledged. We would like to thank V. Kataev for useful discussions and M. Haider for technical support. In particular we are indebted to W. Weber for his ongoing interest and for encouraging us to study this system in more detail.

*Present address: Department of Physics, Graduate School of Science, Kyoto University, Kyoto 606-8502, Japan

[1] J. G. Bednorz and K. A. Müller, Z. Phys. B: Condens. Matter **64**, 189 (1986).
[2] M. F. Collins and O. A. Petrenko, Can. J. Phys. **75**, 605 (1997).
[3] M. Bieringer, J. E. Greedan, and G. M. Luke, Phys. Rev. B **62**, 6521 (2000).
[4] N. Rogado, Q. Huang, J. W. Lynn, A. P. Ramirez, D. Huse, and R. J. Cava, Phys. Rev. B **65**, 144443 (2002).
[5] H. M. Rønnow, A. R. Wildes, and S. T. Bramwell, Physica B **276-278**, 676 (2000).
[6] M. Heinrich, H.-A. Krug von Nidda, A. Loidl, N. Rogado, and R. J. Cava, Phys. Rev. Lett. **91**, 137601 (2003).
[7] S. Shamoto, T. Kato, Y. Ono, Y. Miyazaki, K. Ohoyama, M. Ohashi, Y. Yamaguchi, and T. Kajitani, Physica C **306**, 7 (1998).
[8] R. Weht, A. Filipetti, and W. E. Pickett, Europhys. Lett. **48**, 320 (1999).
[9] V. Kataev, A. Möller, U. Löw, W. Jung, N. Schittner, M. Kriener, and A. Freimuth, J. Magn. Magn. Mater. **290-291**, 310 (2005).
[10] D. A. VanderGriend, S. Boudin, V. Caignaert, K. R. Poeppelmeier, Y. Wang, V. P. Dravid, M. Azuma, M. Takano, Z. Hu, and J. D. Jorgensen, J. Am. Chem. Soc. **121**, 4787 (1999).
[11] M. Azuma, T. Odaka, M. Takano, D. A. VanderGriend, K. R. Poeppelmeier, Y. Narumi, K. Kindo, Y. Mizuno, and S. Maekawa, Phys. Rev. B **62**, R3588 (2000).
[12] Y. Qiu, C. Broholm, S. Ishiwata, M. Azuma, M. Takano, R. Bewley, and W. J. L. Buyers, Phys. Rev. B **71**, 214439 (2005).
[13] S. Malo, D. A. VanderGriend, K. R. Poeppelmeier, Y. Wang, and V. P. Dravid, Solid State Sci. **3**, 17 (2001).
[14] M. T. Anderson, K. B. Greenwood, G. A. Taylor, and K. R. Poeppelmeier, Prog. Solid State Chem. **22**, 197 (1993).
[15] C. Krywka, M. Paulus, C. Sternemann, M. Volmer, A. Remhof, G. Nowak, A. Nefedov, B. Pöter, M. Spiegel, and M. Tolan, J. Synchrotron Radiat. **13**, 8 (2006).
[16] R. Pott and R. Schefzyk, J. Phys. E **16**, 444 (1983).
[17] J. Rodriguez-Carvajal, FULLPROF2000, Version 3.30, June 2005, Laboratoire Léon Brillouin CEA-CNRS, Gif-sur-Yvette, Cedex, France, 2005 (http://www.ill.eu/sites/fullprof/).
[18] Single crystal data $P6_3/mmc$, $Z=2$, $a=3.3564(8)$ Å, $c=11.908(3)$ Å, Mo K_α, $3.42° \leq \Theta \leq 34.95°$, $R_{\text{int}}=0.0627$, $R_1=0.0231$, and $wR2=0.0463$ for all data, z parameter for O^a: 0.0870(4), anisotropic displacement factors (U_{11}, U_{33}, U_{12}, and $U_{\text{eq.}}$ in Å^2) for O^a: 0.007(1), 0.007(2), 0.0034(6), and 0.0068(8), and O^e: 0.039(4), 0.009(3), 0.019(2), and 0.029(2). Note, that the thermal ellipsoids for the metal sites are almost isotropic.
[19] E. F. Bertaut, and J. Mareschal, C. R. Acad. Sci. URSS **275**, 867 (1963).
[20] K. Lukaszewicz and J. Karut-Kalicinska, Ferroelectrics **7**, 81 (1974).
[21] T. Lonkai, D. G. Tomuta, U. Amann, J. Ihringer, R. W. A. Hendrikx, D. M. Többens, and J. A. Mydosh, Phys. Rev. B **69**, 134108 (2004).
[22] J. Weidlein, U. Müller, and K. Dehnike, *Schwingungsspektroskopie* (Thieme Verlag, Stuttgart, 1988).
[23] K. Nakamoto, *Infrared and Raman Spectra of Inorganic and Coordination Compounds* (Wiley, New Jersey, 1978).
[24] M. N. Iliev, H.-G. Lee, V. N. Popov, M. V. Abrashev, A. Hamed, R. L. Meng, and C. W. Chu, Phys. Rev. B **56**, 2488 (1997).
[25] D. G. Tomuta, S. Ramakrishnan, G. J. Nieuwenhuys, and J. A. Mydosh, J. Phys.: Condens. Matter **13**, 4543 (2001).
[26] B. Figgis and M. Hitchman, *Ligand Field Theory and Its Applications* (Wiley, New York, 2000).
[27] D. W. Smith, Inorg. Chim. Acta **22**, 107 (1977).
[28] A. Kutoglu, A. Roesler, and D. Reinen, Z. Anorg. Allg. Chem. **456**, 130 (1979).
[29] We have chosen the two-dimensional centrosymmetric space-group $p31m$ for our results obtained from diffraction experiments. The asymmetric space-group $p3m1$ with the same lattice constants would give two distinct copper sites providing a description for an antiferromagnetic order. In this scenario one would expect an increase in intensity of the structural Bragg peaks. Since this is not observed here, we report the structural centrosymmetric space-group $p31m$.
[30] B. E. Warren, Phys. Rev. **59**, 693 (1941).
[31] The quantum-Monte Carlo data for the (magnetic) internal energy, $U_m(T)$, are reliable in the whole temperature range. This allowed us to determine the coefficient, A, in the spin-wave approximation $U_m(T)=A(\frac{T}{J})^3$ by fitting the Monte Carlo data at low temperatures, [Eq. (5)]. Here we found that the deviations from the T^3 behavior for $U_m(T)$ are small for $T/J<0.15$ but

quickly grow for larger T/J. This means that with $J_{AF}=120$ K, a T^2 behavior for $c_m(T)$ is only valid below $T_{\max.}\sim 18$ K.

[32] K. Fabricius, A. Klümper, U. Löw, B. Büchner, T. Lorenz, G. Dhaleene, and A. Revcolevschi, Phys. Rev. B **57**, 1102 (1998).

[33] The three Θ_E values have been estimated from the IR spectroscopy to be $\approx$160, 350, and 710 K. The first value corresponds to the heaviest metal cation (In), the second belongs to Cu, and the third to V with increasing contributions of oxygen (ratio 1:1.667:2.333). In the very low-temperature limit (below 12 K), we obtained $\Theta_D=268$ K from a linear fit to c_P/T^2. In order to describe the phonon contribution to the specific heat in the whole temperature range, we combine the Debye and Einstein contributions using the following weights $c_{\text{phon}}=c_{\Theta_D}+0.333\ c_{\Theta_{E1}}+0.8\cdot 1.667\ c_{\Theta_{E2}}+2.333\ c_{\Theta_{E3}}$.

[34] B. B. Beard and U.-J. Wiese, Phys. Rev. Lett. **77**, 5130 (1996).

[35] J. D. Reger, J. A. Riera, and A. P. Young, J. Phys.: Condens. Matter **1**, 1855 (1989).

[36] R. F. Bishop and J. Rosenfeld, Int. J. Mod. Phys. B **12**, 2371 (1998).

[37] H.-Q. Ding and M. S. Makivić, Phys. Rev. Lett. **64**, 1449 (1990).

[38] M.-K. Singh, W. Prellier, M. P. Singh, R. S. Katiyar, and J. F. Scott, Phys. Rev. B **77**, 144403 (2008).